

# The ILIAMS project - an RFQ ion beam cooler for selective laser photodetachment at VERA

Martin Martschini<sup>1,‡</sup>, Dag Hanstorp<sup>2</sup>, Johannes Lachner<sup>1</sup>, Christoph Marek<sup>1</sup>, Alfred Priller<sup>1</sup>,  
Peter Steier<sup>1</sup>, Paul Wasserburger<sup>1</sup>, Robin Golser<sup>1</sup>

<sup>1</sup> University of Vienna, Faculty of Physics – Isotope Physics,  
A-1090 Vienna, Austria

<sup>2</sup> Department of Physics, University of Gothenburg, SE-412 96 Gothenburg, Sweden

<sup>‡</sup>Corresponding author: martin.martschini@univie.ac.at

Keywords: AMS; ion beam cooling; selective laser photodetachment; negative ions; isobar suppression;

## Abstract

Selective laser photodetachment of anions is a novel technique for isobar suppression in Accelerator Mass Spectrometry (AMS). Ion-laser interaction times on the order of ms required for near-complete isobar suppression are achieved by retarding the ions in a gas-filled radio frequency quadrupole cooler. Inside this RFQ, the cooled anion beam is overlapped collinearly with an intense cw-laser beam. Within the Ion Laser InterAction Mass Spectrometry (ILIAMS) project at the University of Vienna, a dedicated injector beamline has been coupled to the VERA-AMS facility to explore and develop this method. In this work, experimental investigations on ion beam transmission, stability and elemental selectivity of the new setup are presented.

A 532 nm laser at 10 W transmitted power provides suppression factors larger than ten orders of magnitude for  $S^-$  and  $MgO^-$  under AMS conditions with simultaneous beam transmission for the ions of interest of up to 80%. The excellent ion identification capabilities of the subsequent AMS system also facilitate the study of destruction and formation of molecular anions inside the ion cooler. These kinetic and chemical reactions with the buffer gas provide additional elemental selectivity in certain cases, whereas others constitute a source of background.

## 1. Introduction

1 The idea to use the element selective process of laser photodetachment as a new means of  
2 isobar suppression in AMS was first explored almost 30 years ago [1]. This development was  
3 driven by the aim to overcome the  $\Delta Z/Z$ - and velocity-dependence of established isobar  
4 separation techniques (cf. [2]) preventing measurements of high- $Z$  trace isotopes at  
5 environmental levels. However, it was not until the use of an RFQ ion cooler for anions that  
6 laser ion beam interaction times became sufficiently long to facilitate continuous macroscopic  
7 depletion of interfering ion species using commercially available lasers [3, 4].

8 The main prerequisite of this technique, which is called Ion Laser InterAction Mass  
9 Spectrometry (ILIAMS) in the following, is that the electron affinity EA of the ion of interest  
10 has to be higher than EAs of disturbing ions. This can be fulfilled in either the atomic or a  
11 molecular anion system. Once such a system has been identified, cw-lasers with suitable  
12 photon energy are in general readily available due to big differences in EAs [5,6].  
13 Furthermore, demands on the laser system other than power and beam quality are rather low,  
14 i.e. linewidth and wavelength stability are generally of no concern since photodetachment is a  
15 non-resonant threshold process. After an interaction time  $t$  between ions and a laser beam with  
16 photon flux  $\Phi$ , the number  $N(t)$  of surviving ions with EAs smaller than the photon energy is  
17 simply given by

$$18 N(t) = N(0) \cdot e^{-\sigma \Phi t} \quad (1)$$

19 where  $N(0)$  is the initial number of ions and  $\sigma$  the photodetachment cross section.

20 Assuming a photon flux on the order of  $10^{21} \text{ cm}^{-2} \text{ s}^{-1}$  and typical photodetachment cross  
21 sections around  $10^{-17} \text{ cm}^2$ , efficient removal of isobars to AMS-relevant levels requires  
22 interaction times of at least several hundred of  $\mu\text{s}$ . At the same time, losses of the ions of  
23 interest need to be kept to a minimum.

24 At the University of Vienna, an RFQ ion cooler for selective laser photodetachment of  
25 negative ions has been developed [7]. In the following we will report on the coupling of this  
26 RFQ to the Vienna Environmental Research Accelerator (VERA) AMS facility as part of a  
27 new injection beamline and experimental results.

## 2. Methods

28 A comprehensive description of VERA is found in [8-10]. In this contribution only details of  
29 the new injection beamline of the ILIAMS setup as well as the performance of the RFQ ion  
30 cooler therein will be presented.

Figure 1 shows a schematic of the new injection beamline and the entire VERA AMS-facility.

The major components of the new injector are a 40-sample-MC-SNICS ion source, a double-focussing  $90^\circ$  bending magnet with a bending radius of 0.35 m, an RFQ ion cooler and a set of  $45^\circ$  spherical Electrostatic Analyzers to couple the beam into a standard AMS-injector. The ion energy in the ILIAMS injector is limited to 30 keV by the design of the ion cooler. Hence, the maximum bending power of the  $90^\circ$  magnet of 8.4 MeV amu is sufficient to bend ions up to mass 280 at full injection energy. The image distance of the magnet is such that the nominal beam waist lies exactly at the cooler entrance. Electrostatic xy-steerers before and after the bending magnet allow to adjust ion beam position and direction at the cooler entrance. A Conidur® fine hole sheet made of stainless steel (Hein, Lehmann GmbH, Krefeld, Germany) acts as a 60-fold beam attenuator. The fine perforation of 0.05 mm at a sheet thickness of only 0.2 mm allows thinning out the ion beam without substantially reducing its phase space envelope. This attenuator is employed during injection of the stable reference beam into the ion cooler (cf. 3.1). The long beamline section following the ESA after the ion cooler is due to constraints in the available laboratory space.

The RFQ ion cooler itself has been extensively described in [7], so only its major features are covered here. Its central part is a 951 mm long quadrupole electrode structure terminated by insulated 3 mm apertures at both ends. The radius inscribed by the quadrupole rods is 4.35 mm. A weak longitudinal DC guiding field of typically 2 V/m (maximum 15 V/m) is created by four long plate electrodes wedged in between the RF-rods. A set of aperture lenses counteracts beam expansion during deceleration and allows focusing of the beam during reacceleration. Ion residence times inside the RFQ range from 500  $\mu$ s to several tens of ms depending on injected ion current. The buffer gas pressure, which under routine operation is pure Helium (Air Liquide, class 5), is leaked in at the center of the cooler tube via a manually operated bleeding valve. The entire cooler structure is set to a potential a few ten Volt below the cathode potential in the ion source to facilitate electrostatic deceleration of the ions. Currently, this is achieved by a separate HV-power supply. A difference-stabilized HV-setup is foreseen in the future.

The RF is supplied by two resonant circuits coiled in opposite direction, which are driven via a ferrite transformer by a 200 W E&I 1020L RF power amplifier (Electronics & Innovation Ltd., Rochester, NY, USA) and a function generator DS345 (Stanford Research Systems, Sunnyvale, CA, USA). A binary set of 9 purpose-built switchable inductors ensures resonance conditions for different frequencies. Typically, below 10 W of RF power is necessary to achieve zero-to-peak-voltages of around 300 V at frequencies of a few MHz. However,

1  
2 around 30 W of primary power are required due to significant power reflection at the ferrite  
3 transformer.

4 The entire cw laser setup fits onto a 1.5x1 m laser table placed adjacent to the beamline. The  
5 view port of the bending magnet in cooler direction is equipped with a MgF<sub>2</sub> window to allow  
6 laser beams of wavelengths between 200 nm and 6 μm to enter with > 94% transmission.  
7 Likewise, the 45° ESA after the ion cooler has an 8 mm hole in its outer half-sphere and a  
8 MgF<sub>2</sub> window at the viewport to allow the laser beam to exit. Commercial calorimetric power  
9 meters are used to monitor the transmitted laser power. Until now, all experiments have been  
10 conducted with a 532 nm 18 W VERDI-V18 cw laser (Coherent Inc, Santa Clara, CA, USA),  
11 but a 984 nm (10 W) and a tunable IR 2000-3000 nm (<5 W) are also available in the  
12 laboratory.  
13

14 All components including the cw laser have been fully integrated into the VERA control  
15 system “*AccelNET*” (NEC, Middleton, WI, USA) via a separate Beckhoff control system  
16 (Beckhoff Automation GmbH & Co. KG, Verl, Germany) and a parameter exchange server  
17 developed in-house. This allows to operate ILIAMS and VERA remotely and to run fully-  
18 automated measurements.  
19

20 The absence of slits at the beam waist between the ILIAMS magnet and the RFQ ion cooler  
21 unfortunately limits the mass resolution of the setup in its present state to  $m/\Delta m \approx 150$ .  
22 Figure 2 shows a simulation with SIMION 8.1 (Scientific Instrument Services, Inc., Ringoes,  
23 NJ, USA) of neighboring beams at masses 273 to 277. In combination with the injection lens  
24 system, the separation of the different mass beams is too small to fully block the neighboring  
25 beams by the 3 mm entrance aperture or any of the preceding aperture lenses. This is also  
26 observed experimentally when injecting HfF<sub>5</sub><sup>-</sup> and WF<sub>5</sub><sup>-</sup> into the ion cooler (cf. Figure 4).  
27 With all components optimized for injection of mass 277 (<sup>182</sup>WF<sub>5</sub><sup>-</sup>), about 1% of <sup>180</sup>HfF<sub>5</sub><sup>-</sup>  
28 (m=275) is still transmitted. Based on detailed studies of the ion optics, additional x-slits will  
29 be mounted between magnet and ion cooler to overcome this problem.  
30  
31  
32  
33  
34  
35  
36  
37  
38  
39  
40  
41  
42  
43  
44  
45  
46  
47  
48

### 49 **3. Results and Discussion**

#### 50 3.1 Transmission and stability

51 Among the major prerequisites of AMS is that unknown sample and reference sample are  
52 measured under identical conditions, implying that the total ion detection efficiencies both for  
53 stable and rare isotopes are constant. Slight current dependencies of measured isotopic ratios  
54 are nevertheless observed at many AMS facilities (e.g. [11]) and usually attributed to small  
55 variations in accelerator transmission. Unfortunately, the RFQ-ion cooler exhibits a strong  
56  
57  
58  
59  
60  
61  
62  
63  
64  
65

1 variation in transmission with ion current when stable reference isotope beams of several  $\mu\text{A}$   
2 are injected. These are however often required in AMS in order to reach sufficient statistics of  
3 the rare isotope within reasonable time. This current-dependency of the RFQ has already been  
4 discussed in [7]. Higher ion currents lead to increased phase space of the ion beam when  
5 leaving the ion source and shorter residence times inside the RFQ. Furthermore, losses inside  
6 the RFQ increase as the stored charge approaches the charge limit of the RFQ and ions are  
7 increasingly getting pushed out of the potential well by space charge. Also the RF-heating of  
8 stored ions is growing once they are pushed away from the potential minimum in the cooler  
9 axis by space charge, resulting in higher ion energy spreads.

10 As these are fundamental limitations, no changes in this behavior were expected with  
11 integration of the cooler into the new injector. This is confirmed by transmission data for  
12 various  $^{37}\text{Cl}^-$ -currents in the  $\mu\text{A}$  range shown in Figure 3a. They were recorded during a  
13 routine AMS measurement with the ILIAMS setup lasting over 48 hours. To overcome the  
14 problem of current dependency of ratios, a phase space conserving beam attenuator is now  
15 employed to reduce the intensity of the stable reference isotope beam by a factor of 60.  
16 Figure 3b shows the transmission of the attenuated  $^{37}\text{Cl}^-$  ion beams for the same set of data.  
17 With injected ion currents of only several tens of nA no more current dependency of  
18 transmission is observed. The reproducibility of individual samples in routine AMS  
19 measurements with normalization to the attenuated stable isotope is better than 3% and the  
20 whole system including the laser was tested to be stable over several days. The attenuator is  
21 inserted via a motorized translator, which takes roughly 5 s. This limits the minimum  
22 switching time between stable isotope and rare isotope ion beams. More details on  
23 measurement strategy and results of the first AMS-measurements of  $^{36}\text{Cl}$  with ILIAMS can be  
24 found in [12].

### 25 3.2 Isobar suppression – fragmentation and formation of molecules:

26 The behavior of the RFQ cooler for the molecular anion system  $\text{MgO}^-$  and  $\text{AlO}^-$  has already  
27 been investigated on the ILIAS test bench [7]. However, this setup did not provide any mass  
28 analysis of the transmitted ion current. Hence, only upper limits for the isobar suppression  
29 factors based on the total ejected ion current could be given. The mass-composition of the  
30 extracted ion beam and the fraction of the anion under investigation therein could not be  
31 determined. Nevertheless, a suppression factor of  $>10^4$  for  $\text{MgO}^-$  vs  $\text{AlO}^-$  could be  
32 demonstrated at 10.8 W transmitted power of the 532 nm laser [7].

1 The new ILIAMS setup benefits from the full mass analysis of the VERA injector and, if  
2 necessary, the entire subsequent AMS facility. This allows a detailed analysis of the  
3 composition of the ejected negative ion beam. Interestingly, fragmentation and formation of  
4 molecules as well as pickup of fragments by injected ions are all observed in pure He buffer  
5 gas. Figure 4a shows mass spectra obtained when injecting  $\text{AlO}^-$  at mass 43,  $\text{MgO}^-$  at mass 40  
6 and 41 as well as  $^{37}\text{Cl}^-$  into the ion cooler without laser light. The distinct peaks at masses 16  
7 and 17 when injecting  $\text{AlO}^-$  and  $\text{MgO}^-$  clearly show that  $^{16}\text{O}^-$  and  $^{16}\text{OH}^-$  are both formed  
8 when oxygen-containing anions are injected. Since these ions have no stable trajectories  
9 inside the RFQ under routine operating conditions for masses around 40, the ion cooler was  
10 specifically set for the low masses. While the ILIAMS RFQ is not operated as a quadrupole  
11 mass filter but as an ion guide (i.e. no DC voltage is applied to the RF electrodes), only ions  
12 within roughly  $\pm 30\%$  mass deviation from the tuned ion mass are efficiently transported  
13 through the RFQ for a given RF frequency and amplitude (see [7] for details and experimental  
14 data). Hence, the transmission for the injected masses 37 to 43 was below 1% during these  
15 experiments with RFQ settings optimized for ions around mass 16. The injector mass scans in  
16 Figure 4a were recorded using a Faraday cup placed directly after the accelerator for  
17 enhanced mass resolution. The plotted currents are thus convoluted with the charge state  
18 distribution of each ion species. The fact that the ratio between  $\text{O}^-$  and  $\text{OH}^-$  changes by almost  
19 an order of magnitude when injecting mass 41 ( $^{25}\text{MgO}^-$  and  $^{24}\text{MgOH}^-$ ) instead of 40 ( $^{24}\text{MgO}^-$ )  
20 is a very strong indication that injected elements rather than impurities in the He buffer gas  
21 are the main source for these anion species. Both scans were conducted from the same sputter  
22 sample after more than an hour of presputtering and less than 15 min apart. The only  
23 parameter changed was the ILIAMS magnet, which was switched from mass 40 to 41.  
24 Another interesting feature is the peak at mass 32, which was observed when injecting  $1.5 \mu\text{A}$   
25 of  $\text{AlO}^-$ . The same peak appeared in mass scans when injecting  $^{24}\text{MgO}^-$  and tuning the ion  
26 cooler for mass 32. This peak indeed belongs to  $\text{O}_2^-$ , which was confirmed by identification of  
27  $^{16}\text{O}^+$ ,  $^{16}\text{O}^{2+}$  and  $^{16}\text{O}^{3+}$  after VERA's high-energy-side analyzing magnet and the absence of  
28 any other noticeable peak. We attribute this to the formation of  $\text{O}_2^-$  from single O and  $\text{O}^-$   
29 originating from the dissociation of injected anions. As a quick verification experiment, also  
30  $^{16}\text{O}^-$  was injected into the ion cooler and resulted in the formation of 10 pA of mass 32. A  
31  $^{37}\text{Cl}^-$  beam in the ion cooler produces no peaks above background at lower masses.

32 Buffer gases other than He enhance certain reactions or provide reaction partners. These  
33 processes may boost elemental selectivity in addition to laser photodetachment but are  
34 possible sources of background as well. Negative ion gas reactions have been studied at eV  
35  
36  
37  
38  
39  
40  
41  
42  
43  
44  
45  
46  
47  
48  
49  
50  
51  
52  
53  
54  
55  
56  
57  
58  
59  
60  
61  
62  
63  
64  
65

1 energies at University of Toronto in a similar RFQ setup, which aims at isobar separation for  
2 AMS solely by reactions of anions with buffer gas [13]. They report e.g. on the identification  
3 of  $\text{YF}_3\text{O}^-$  after the RFQ when injecting  $\text{YF}_3^-$  into  $\text{NO}_2$  buffer gas. Furthermore, a strong  
4 suppression of  $\text{WF}_5^-$  versus  $\text{HfF}_5^-$  was observed in  $\text{O}_2$  buffer gas [14]. This was attributed to  
5 the formation of oxyfluorides, although the exact processes remained elusive. Since such  
6 technique may enable measurements of the astrophysically interesting trace isotope  $^{182}\text{Hf}$   
7 [15,16], we decided to investigate the behavior of  $^{182}\text{WF}_5^-$  in different buffer gas mixtures by  
8 mass analysis of the ejected ion current. The results are shown in Figure 4b. The sputter target  
9 used for this experiment was a 1:1:1 by weight mixture of  $\text{HfF}_4$ , W and  $\text{PbF}_2$ . The ILIAMS  
10 magnet was set for mass 277 although, as already mentioned above, the mass resolution of the  
11 setup in its present state is too low to fully suppress neighboring masses. Hence a distinct  
12 peak at mass 278 (mostly  $^{183}\text{WfF}_5^-$ ) and even a small fraction of the much more intense  
13  $^{180}\text{HfF}_5^-$  peak (mass 275) is still visible in the spectrum. The different buffer gases were  
14 premixed in a small pressure bottle, which lasted for about 10 hours of operation at the typical  
15 buffer gas pressure of 0.25 mbar. This was more than sufficient as each mass scan in  
16 Figure 4b lasted less than 10 min, after which the buffer gas was exchanged. The dominant  
17 process is the pickup of O to form  $^{182}\text{WF}_5\text{O}^-$ , which even occurs at a noticeable rate in pure  
18 He (nominal purity  $\geq 99.999$  mol%). Addition of 1%  $\text{N}_2$  to the He gas results in a clearly  
19 increased reaction rate, the original beam is reduced by  $\sim 30\%$ . While there is  $\sim 40$  pA less  
20  $^{182}\text{WF}_5^-$ , the peak at mass 293 attributed to  $^{182}\text{WF}_5\text{O}^-$  increases by just the same amount. The  
21 source of O for this process is likely to be O-containing molecules around mass 277. The  
22 presence of heavier collision partners in the form of  $\text{N}_2$  buffer gas presumably leads to an  
23 increased destruction rate of these molecules and provides more reaction partners for  $^{182}\text{WF}_5^-$ .  
24 Deliberate addition of 1%  $\text{O}_2$  to pure He buffer gas further enhances this reaction channel  
25 with  $>75\%$  of the  $^{182}\text{WF}_5^-$  transformed into  $^{182}\text{WF}_5\text{O}^-$ . At higher  $\text{O}_2$  levels of 10% in the  
26 buffer gas, no more  $^{182}\text{WF}_5^-$  is ejected from the RFQ. At the same time, also  $^{182}\text{WF}_5\text{O}^-$  is now  
27 strongly reduced indicating either some further reaction to masses outside the investigated  
28 range or neutralization of these anions. The formation of  $^{182}\text{WF}_4\text{O}^-$  was not observed in any of  
29 the buffer gases. In analogy to  $\text{WF}_5\text{O}^-$ , also the formation of  $\text{HfF}_3\text{O}^-$  from  $\text{HfF}_3^-$  in He buffer  
30 gas has been experimentally verified.

31 While reactions of isobaric molecular anion species are generally beneficial, there are also  
32 cases of the opposite. This happens, e.g., when molecular reactions contribute to the  
33 transmission of anions by evading selective photodetachment through quick enough  
34 transmutation once entering the laser interaction region in the RFQ. One example would be  
35  
36  
37  
38  
39  
40  
41  
42  
43  
44  
45  
46  
47  
48  
49  
50  
51  
52  
53  
54  
55  
56  
57  
58  
59  
60  
61  
62  
63  
64  
65

1  $C_3^-$  with an electron affinity EA of 1.995(25) eV [6], which is easily detached by our 2.33 eV  
2 Verdi laser during  $^{36}\text{Cl}$  measurements. Collisions of  $C_3^-$  with pure He buffer gas can however  
3 result in the transmutation into  $C_2^-$  [12]. With an EA of 3.269(6) eV [6], this anion is immune  
4 against photodetachment by 2.33 eV photons. The reaction rate increases with ion injection  
5 energy into the buffer gas. In the absence of any mass filter between the RFQ cooler and  
6 injection into the accelerator, such processes may contribute to background in the final  
7 detection setup. With all these new results at hand, we started to assess isobar suppression  
8 factors in the RFQ cooler by both laser photodetachment and possible molecular reactions  
9 combined. Table 1 contains suppression factors recently achieved with our setup for three  
10 anion systems of interest for AMS. In most cases it was even necessary to deliberately spike  
11 test samples with isobaric contamination like MgO or S at the % level in order to determine  
12 the isobar suppression factor of the ILIAMS setup. Given the 10+ orders of magnitude  
13 suppression both for  $\text{MgO}^-$  vs.  $\text{AlO}^-$  and  $\text{S}^-$  vs.  $\text{Cl}^-$ , any further atomic isobar suppression in  
14 the detection system for these elements becomes obsolete. Thus, low charge states with high  
15 stripping yields can be employed. The full experimental details on the benefits and  
16 implications of this novel technique for  $^{36}\text{Cl}$  AMS measurements at VERA are presented in  
17 [12].  
18  
19  
20  
21  
22  
23  
24  
25  
26  
27  
28  
29  
30

#### 31 **4. Conclusions and Outlook**

32 The ILIAMS setup has been fully integrated into the VERA facility, which now allows  
33 studies of isobar suppression by laser photodetachment at AMS sensitivity levels. The entire  
34 setup has been tested to be stable over several days of measurement and opens ample  
35 possibilities for studies of element-selective photodetachment as well as reactions of  
36 molecules with buffer gas and ambient molecular fragments at eV energies. Given the  
37 experimental results, we emphasize the importance of a mass filter after the RFQ prior to  
38 injection of the ion beam into the accelerator in order to achieve highest isobar suppression.  
39

40 Further experiments are foreseen to investigate the degree of  $\text{WF}_5^-$  vs  $\text{HfF}_5^-$  suppression in a  
41 He- $\text{O}_2$  buffer gas to determine the feasibility of  $^{182}\text{Hf}$  measurements. This anion system also  
42 illustrates one of the main experimental challenges of this novel technique regarding new  
43 trace isotopes: The electron affinities of many molecular anion species are still unknown or  
44 only theoretical calculations exist. Hence selection of an appropriate molecular system and  
45 corresponding cw-laser requires some experimental studies. In the case of Hafnium- and  
46 Tungsten-pentafluorides, the only experimental stake so far is the finding that the  
47  
48  
49  
50  
51  
52  
53  
54  
55  
56  
57  
58  
59  
60  
61  
62  
63  
64  
65



1 photodetachment cross section for  $\text{WF}_5^-$  is a factor of 100 higher than for  $\text{HfF}_5^-$  at 266 nm  
2 [17].

3 In addition to the scarcity of electron affinity data, kinetic and chemical reactions of  
4 molecular anions in the RFQ may strongly enhance isobar suppression, but could also render  
5 certain anion species unsuitable for this technique. Among the promising candidates for  
6 applications of the ILIAMS technique in the near future are  $^{53}\text{MnO}^-$  (1.375(10) [18]) /  $^{53}\text{CrO}^-$   
7 (1.221(6) [6]),  $^{60}\text{FeH}^-$  (0.481(7) [6]) /  $^{60}\text{NiH}^-$  (0.481(7) [6]),  $^{93}\text{ZrF}_5^-$  /  $^{93}\text{NbF}_5^-$  (experimental  
8 EA values given in eV where known).  
9  
10  
11  
12  
13  
14  
15

### 16 **Acknowledgments**

17  
18 This work was supported by the University of Vienna (Investitionsprojekte 2012, 2013, 2015,  
19 2016, 2017). DH acknowledges support from the Swedish Research Council.  
20  
21  
22  
23

### 24 **References:**

- 25  
26 [1] D. Berkovits, E. Boaretto, G. Hollos, W. Kutschera, R. Naaman, M. Paul and Z. Vager,  
27 Nucl. Instrum. Methods A 281 (1989) 663.  
28  
29 [2] H.A. Synal, Int. J. Mass Spectrom. 349-350 (2013) 192.  
30  
31 [3] Y. Liu, J.R. Beene, C.C. Havener and J.F. Liang, Appl. Phys. Lett. 87 (2005) 113504.  
32  
33 [4] P. Andersson, A.O. Lindahl, D. Hanstorp, C.C. Havener, Y Liu and Y Liu, J. Appl. Phys.  
34 107 (2010) 026102.  
35  
36 [5] T. Andersen, H. Haugen and H. Hotop, J. Phys. Chem. Ref. Data 28 (6) (1999) 1511.  
37  
38 [6] J.C. Rienstra-Kiracofe, G.S. Tschumper, H.F. Schaefer, S. Nandi and G.B. Ellison, Chem.  
39 Rev. 102 (2002) 231.  
40  
41 [7] M. Martschini, J. Pitters, T. Moreau, P. Andersson, O. Forstner, D. Hanstorp, J. Lachner,  
42 Y. Liu, A. Priller, P. Steier and R. Golser, Int. J. Mass Spectrom. 415 (2017) 9.  
43  
44 [8] C. Vockenhuber, I. Ahmad, R. Golser, W. Kutschera, V. Liechtenstein, A. Priller, P. Steier  
45 and S. Winkler, Int. J. Mass Spectrom. 223–224 (2003) 713.  
46  
47 [9] P. Steier, R. Golser, W. Kutschera, A. Priller, C. Vockenhuber and S. Winkler, Nucl.  
48 Instrum. Methods B 223–224 (2004) 67.  
49  
50 [10] A. Priller, K. Melber, O. Forstner, R. Golser, W. Kutschera, P. Steier and A. Wallner,  
51 Nucl. Instrum. Methods B 268 (7–8) (2010) 824.  
52  
53 [11] P.W. Kubik and M. Christl, Nucl. Instrum. Methods B 268 (2010) 880.  
54  
55  
56  
57  
58  
59  
60  
61  
62  
63  
64  
65

1 [12] J. Lachner, C. Marek, M. Martschini, A. Priller, P. Steier, and R. Golser, <sup>36</sup>Cl in a new  
2 *light: AMS-measurements assisted by ion-laser interaction*, these proceedings.

3 [13] J.A. Eliades, X.L. Zhao, A.E. Litherland and W.E. Kieser, Nucl. Instrum. Methods B 361  
4 (2015) 294.  
5

6 [14] X.-L. Zhao, J. Eliades, A.E. Litherland, W.E. Kieser, J. Cornett, and C.R.J. Charles,  
7 Rapid Comm. Mass Spectrom. 27 (2013) 2818.  
8

9 [15] C. Vockenhuber, F. Oberli, M. Bichler, I. Ahmad, G. Quitté, M. Meier, A. N. Halliday,  
10 D. C. Lee, W. Kutschera, P. Steier, R. J. Gehrke, R. G. Helmer, Phys. Rev. Lett. 93 (2004)  
11 172501.  
12

13 [16] C. Vockenhuber, C. Feldstein, M. Paul, N. Trubnikov, M. Bichler, R. Golser,  
14 W. Kutschera, A. Priller, P. Steier and S.R. Winkler, New Astron. Rev. 48 (2004) 161.  
15

16 [17] T. Leopold, J. Rohlén, P. Andersson, C. Diehl, M. Eklund, O. Forstner, D. Hanstorp,  
17 H. Hultgren, P. Klason, A.O. Lindahl and K. Wendt, Int. J. Mass Spectrom. 359 (2014) 12.  
18

19 [18] G.L. Gutsev, B.K. Rao, P. Jena, X. Li and L.S. Wang, J. Chem. Phys. 113 (4) (2000)  
20 1473.  
21  
22  
23  
24  
25  
26  
27  
28  
29  
30  
31  
32  
33  
34  
35  
36  
37  
38  
39  
40  
41  
42  
43  
44  
45  
46  
47  
48  
49  
50  
51  
52  
53  
54  
55  
56  
57  
58  
59  
60  
61  
62  
63  
64  
65

Table 1

anions	AMS-isotope	suppr. factor
$\text{MgO}^-$ vs $\text{AlO}^-$ (1.60 eV vs 2.66 eV)	$^{26}\text{Al}$	$10^{11}$
$\text{S}^-$ vs $\text{Cl}^-$ (1.60 eV vs 2.66 eV)	$^{36}\text{Cl}$	$3 \times 10^{10}$
$\text{BaF}_2^-$ vs $\text{CsF}_2^-$ (EAs unknown)	$^{135}\text{Cs}$	$>10^4$

Experimental anion suppression factors by laser photodetachment measured with He-buffer gas and 10 W transmitted laser power at 532 nm (2.33 eV). Where known, experimental electron affinities are given [5,6]

Figure captions:

1  
2 Figure 1: Schematic drawing of the ILIAMS setup and its location within the VERA AMS  
3 facility. Electrostatic components are shown in yellow, magnetic components in blue and  
4 components for ion generation and detection in green.  
5

6  
7 Figure 2: SIMION 8.1 simulation of the injection section of the RFQ ion beam cooler  
8 including the first 5 cm of the RFQ buffer gas section for neighboring mass beams:  $m=273$   
9 (black),  $m=274$  (green),  $m=275$  (red),  $m=276$ (cyan),  $m=277$ (blue). Lateral distances in the top  
10 view plot are magnified by a factor 2. The input ion beam parameters are based on phase  
11 space measurements at the object slits of the ILIAMS magnet. Calculated ion beam  
12 transmissions of 43% ( $m=275$ ), 15% ( $m=274,276$ ) and 1.5% ( $m=273,277$ ) with all injection  
13 components optimized for mass 275 closely match the experimental situation with a mass  
14 resolution of  $m/\Delta m = 150$ .  
15  
16  
17

18  
19 Figure 3: Ion beam transmission of  $^{37}\text{Cl}^-$  through the RFQ ion cooler at 0.31 mbar He as a  
20 function of injected ion currents during 48 hours of  $^{36}\text{Cl}$ -AMS. The injected  $^{37}\text{Cl}^-$  current is  
21 measured in the Faraday cup in front of the RFQ cooler, and the RFQ transmitted  $^{37}\text{Cl}^-$   
22 current is measured in an offset-Faraday cup following VERA's injection magnet (cf.  
23 Figure 1). Data points stem from 20 min runs on different sputter targets, a full turn of the  
24 target wheel takes around 6 h, the start time of each turn is given in the plots. During a 20 min  
25 run, unattenuated and attenuated ion beam transmissions are measured almost simultaneously  
26 (less than 1 min apart) every 5 min. The plotted data points are averages over a run. (a) shows  
27 the current dependency of transmission for the unattenuated stable reference beam as a  
28 function of ion current. (b) shows the transmission values as a function of ion current for the  
29 same set of samples but with the fine hole sheet attenuator inserted. Other than this, no prior  
30 beam collimation out of the ion source is employed.  
31  
32  
33  
34  
35

36  
37 Figure 4: Mass scans of the anion beams ejected from the RFQ with the VERA injection  
38 magnet. (a) Comparison of mass scans with the RFQ optimized for transmission of  $\text{O}^-$  ( $m=16$ )  
39 when injecting  $\text{MgO}^-$ ,  $\text{MgOH}^-$ ,  $\text{AlO}^-$  and  $^{37}\text{Cl}^-$  into pure He buffer gas. Note that the  $^{16}\text{O}^-$   
40 / $^{16}\text{OH}^-$  obviously changes with the amount of H-containing molecules injected. Hence, the  
41 source of hydrogen is unlikely to be impurities in the He buffer gas. (b) Comparison of mass  
42 spectra when injecting mass 277 ( $^{182}\text{WF}_5^-$ ) and tails of neighboring masses into various buffer  
43 gases. Pickup of O by  $\text{WF}_5^-$  to form  $\text{WF}_5\text{O}^-$  is the most prolific reaction observed in this mass  
44 range.  
45  
46  
47  
48  
49  
50  
51  
52  
53  
54  
55  
56  
57  
58  
59  
60  
61  
62  
63  
64  
65

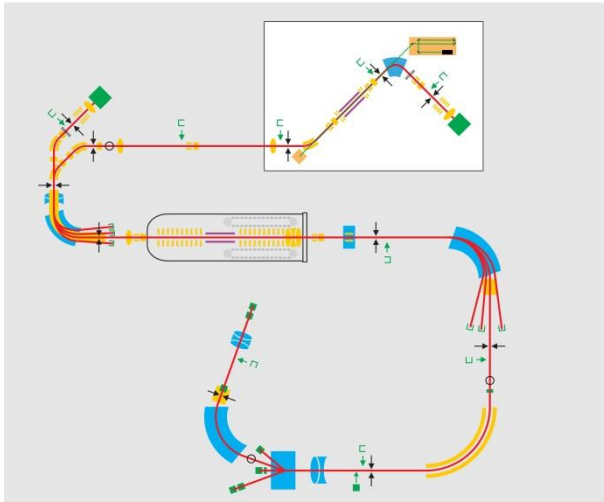
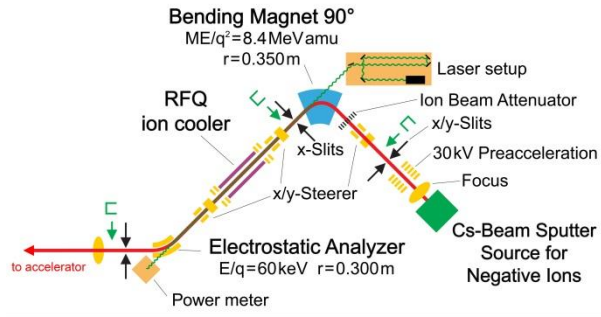


Figure 1

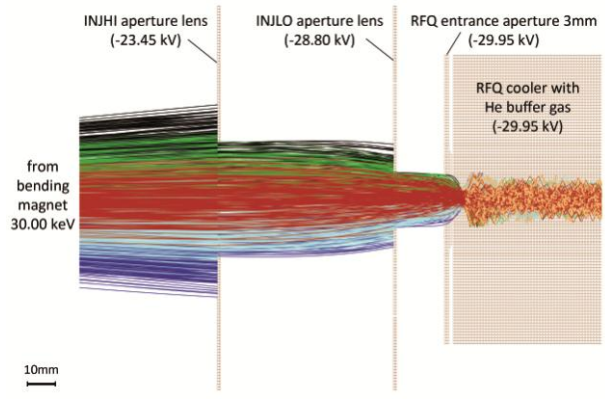
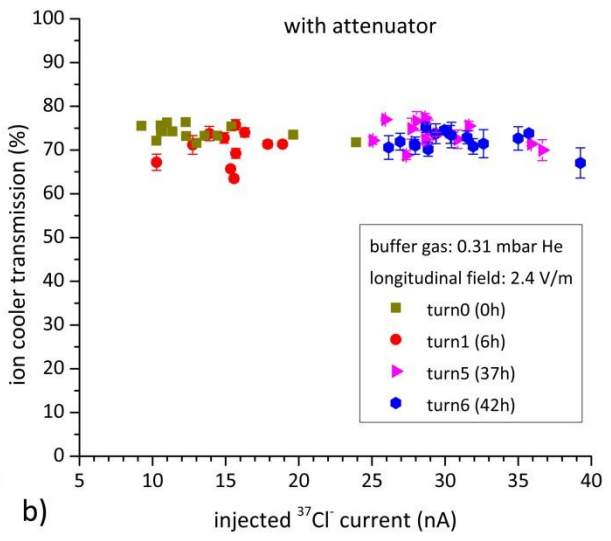
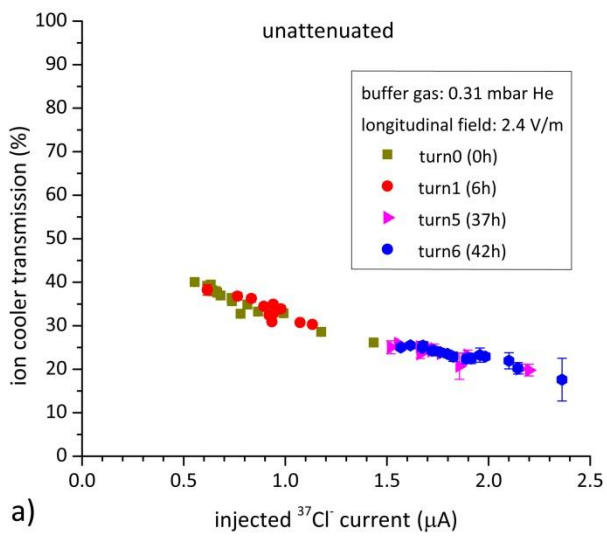
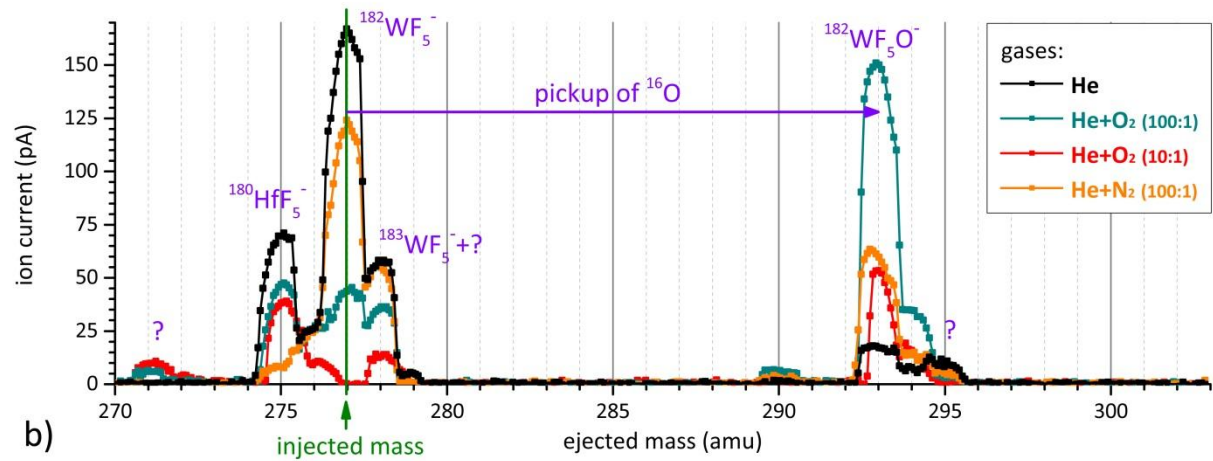
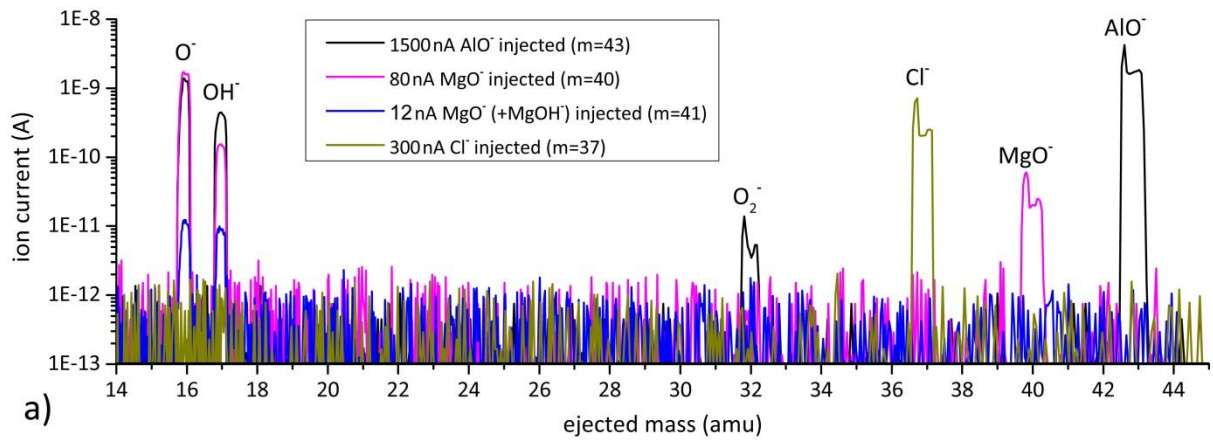


Figure 2



a)  
Figure 3

1  
2  
3  
4  
5  
6  
7  
8  
9  
10  
11  
12  
13  
14  
15  
16  
17  
18  
19  
20  
21  
22  
23  
24  
25  
26  
27  
28  
29  
30  
31  
32  
33  
34  
35  
36  
37  
38  
39  
40  
41  
42  
43  
44  
45  
46  
47  
48  
49  
50  
51  
52  
53  
54  
55  
56  
57  
58  
59  
60  
61  
62  
63  
64  
65



31 Figure 4  
32  
33  
34  
35  
36  
37  
38  
39  
40  
41  
42  
43  
44  
45  
46  
47  
48  
49  
50  
51  
52  
53  
54  
55  
56  
57  
58  
59  
60  
61  
62  
63  
64  
65